JOURNAL OF GEOPHYSICAL RESEARCH, VOL. 104, NO. C7, PAGES 15,495–15,514, JULY 15, 1999

Equatorial currents and transports in the upper central Indian Ocean: Annual cycle and interannual variability

Jörg Reppin, Friedrich A. Schott, and Jürgen Fischer

Institut für Meereskunde, Universität Kiel, Kiel, Germany

Detlef Quadfasel[1]

Institut für Meereskunde, Universität Hamburg, Hamburg, Germany

Abstract. The zonal circulation south of Sri Lanka is an important link for the exchange of water between the Bay of Bengal and the Arabian Sea. Results from a first array of three moorings along 80°30'E north of 4°10'N from January 1991 to March 1992 were used to investigate the Monsoon Current regime [*Schott et al.,* 1994]. Measurements from a second array of six current meter moorings are presented here. This array was deployed along 80°30'E between 45'S and 5°N from July 1993 to September 1994 to investigate the annual cycle and interannual variability of the equatorial currents at this longitude. Both sets of moorings contribute to the Indian Ocean current meter array ICM8 of the World Ocean Circulation Experiment. The semiannual equatorial jet (EJ) was showing a large seasonal asymmetry, reaching a monthly mean eastward transport of 35 Sv (1 Sv $= 1 \times 10^6$ m^3 s^{-1}) in November 1993, but just 5 Sv in May 1994. The Equatorial Undercurrent (EUC) had a maximum transport of 17 Sv in March to April 1994. Unexpectedly, compared to previous observations and model studies, the EUC was reappearing again in August 1994 at more than 10 Sv transport and was still flowing when the moorings were recovered. In addition, monthly mean ship drifts near the equator are evaluated to support the interpretation of the moored observations. Interannual variability of the EJ in our measurements and ship drift data appears to be related to the variability of the zonal winds and Southern Oscillation Index. The output of a global numerical model (Parallel Ocean Climate Model) driven by the winds for 1993/1994 is used to connect our observations to the larger scale. The model reproduces the EJ asymmetry and shows the existence of the EUC and its reappearance during summer 1994.

1. Introduction

The area south of the Indian subcontinent is an important bottleneck for the exchange of water masses between the two northern basins of the Indian Ocean, the Arabian Sea and the Bay of Bengal. A first set of three moorings, part of the Indian Ocean current meter array ICM8 of the World Ocean Circulation Experiment (WOCE), was deployed in this area north of 4°10'N and the coast between January 1991 and March 1992 to study the Monsoon Currents [*Schott et al.,* 1994]. These data revealed a quite shallow Monsoon Current system, decaying rapidly in the vertical in the upper 100 m. While the transport immediately south of Sri Lanka could be well determined from the array observations, it remained unclear how far equatorward the Monsoon Current in either of the monsoon phases would extend. Some speculations were made for the latitude belt 2°- 5°N in that first analysis, based on climatological and ship section data. A second array of current meter moorings was deployed during July 1993 to September 1994, extending the first line across the equator to 0°45'S to investigate the equatorial currents and extend the observations of the Monsoon Current system. The scope of this article is to present and discuss the seasonal cycle of the currents and transports along 80°30'E at and north of the equator from these measurements and to point out some striking anomalies in the equatorial circulation as compared to our prior knowledge from climatological observations.

[1]Now at Niels Bohr Institute for Astronomy, Physics and Geophysics, University of Copenhagen, Copenhagen.

Paper number 1999JC900093.
0148-0227/99/1999JC900093$09.00

The circulation of the northern Indian Ocean is strongly influenced by the reversing monsoons. The most prominent feature is the reversal of the Somali Current at the western boundary during the annual cycle. During the NE monsoon, between November and February, the southward Somali Current carries water from the Arabian Sea across the equator in the near-surface layer [*Schott et al.*, 1990]. Between 2° and 4°S the current meets the East African Coast Current and feeds into the eastward South Equatorial Countercurrent (SECC) [*Düing and Schott*, 1978]. South of Sri Lanka, climatological maps of ship drifts [*Cutler and Swallow*, 1984; *Rao et al.*, 1989] and the measurements from the first set of moorings [*Schott et al.*, 1994] show the Northeast Monsoon Current (NMC) to flow westward during that time. The transport of the shallow NMC was 12 Sv in January/February 1991 and 10 Sv during the same period in 1992. The connection between the western boundary regime off east Africa and the Monsoon Current regime is, so far, unknown. Low-salinity surface waters west and northwest of Sri Lanka originating from the Bay of Bengal during this time [*Wyrtki*, 1971] demonstrate the area to be crucial for the exchange of water between the Bay of Bengal and the Arabian Sea. This is supported by the climatological ship drift data [*Cutler and Swallow*, 1984]. They show southward surface currents along the east coast of India, a westward extension of the NMC in the 2°- 6°N latitude band, and a northward boundary current along the western coast of India. Hydrographic data from December 1987 and January 1988 also showed a 200-m-deep northward boundary current and indications for a southward undercurrent along the west coast of India [*Shetye et al.*, 1991].

During the SW Monsoon (June-September) the cross-equatorial Somali Current flows northward, feeding into the Great Whirl that is located off the coast of Somalia between 5° and 10°N [e.g., *Schott et al.*, 1997; *Fischer et al.*, 1996]. During that time the Southwest Monsoon Current (SMC) south of Sri Lanka flows eastward [*Cutler and Swallow*, 1984; *Schott et al.*, 1994]. The SMC just reaches down to about 100 m depth, as well, and its transport was 8 Sv north of 3°45'N during June 1991. Extending the current to 2°N and using shipboard measurements and ship drift currents resulted in a transport estimate of 15 Sv [*Schott et al.*, 1994]. Hydrographic sections west of India between June and August 1987 revealed a southward surface current within the upper 75 to 100 m with a poleward undercurrent underneath [*Shetye et al.*, 1990]. This is to be expected for the climatological wind stress field and Ekman transport situation during that monsoon phase. On the other hand, geostrophic and direct current measurements along 8°N off the Indian continental slope in August 1993 [*Stramma et al.*, 1996] showed a northward surface boundary current but for a wind situation that differed from the climatology in having a northward component. During the same time a westward current was observed just south of Sri Lanka [*Schott et al.*, 1994], suggesting supply of this northward current. Typically, a northward surface current exists during this time of year along the east coast of India as hydrographic measurements from March and April 1991 [*Shetye et al.*, 1993] and the ship drifts [*Cutler and Swallow*, 1984] indicate.

Model studies [e.g., *McCreary et al.*, 1993] suggest that the currents around India are affected by baroclinic Kelvin waves that propagate around the subcontinent. One of their generation mechanisms is through eastward equatorial Kelvin waves propagating up the eastern Bay of Bengal; and, in fact, such a westward near-coastal pulse, embedded in the eastward SMC, was seen in shipboard observations of July 1993 [*Schott et al.*, 1994].

In the equatorial band covered by the array, two circulation features stand out. During the transition phases between the two monsoons, April/May and October/November, an eastward equatorial jet [*Wyrtki*, 1973] is driven by westerly winds along the equator. It exists throughout the whole zonal extent of the equatorial ocean and reaches current amplitudes of more than 80 cm s^{-1} [*Reverdin*, 1987]. *Visbeck and Schott* [1992] have shown, in an analysis of Geophysical Fluid Dynamics Laboratory (GFDL) model data, that semiannual equatorial waves can explain most of the variance of these jets. They supply the Kelvin wave signals associated with the northern boundary variability of *McCreary et al.* [1993].

Underneath the equatorial jet (EJ), an Equatorial Undercurrent (EUC) exists, but not throughout the whole year as in the Atlantic or Pacific Oceans. Observational evidence on the EUC is scarce. It was shown in equatorial current profiles across the equator between 53° and 92°E in March and April 1963 with speeds of up to 80 cm s^{-1}, while it was not existent during the SW Monsoon [*Taft and Knauss*, 1967]. A nearly 2-year-long time series (January 1973 to October 1974) of equatorial temperature and current profiles within the upper 300 m off the Addu Atoll (73°E) showed the EUC with maximum zonal velocities of about 100 cm s^{-1} during March of the first year, while it was absent during the second year [*Knox*, 1976]. Sections along 55°30'E during February to June 1975 and 1976, again, showed the existence of the undercurrent in both years with speeds of about 80 cm s^{-1} [*Leetmaa and Stommel*, 1980]. The conditions for EUC occurrence, i.e., the setup of an eastward subsurface pressure gradient, were found to depend on the traveling time and reflection of equatorial Kelvin and Rossby waves in response to equatorial wind forcing. The wave mechanism could be used to explain the difference between the 1973 and 1974 observations from the interannual differences in the observed winds [*Cane*, 1980].

In this presentation we show time series of the EJ and EUC transports and find some astonishing deviations from our preconceptions. First, the EJ is anomalously

small in northern spring of 1994 and large in fall 1993; and, second, we find, besides the existence of the EUC during February to June, its reoccurrence into a well-developed state toward the end of the time series, in August/September 1994.

By analyzing the output fields of a numerical model, we relate our observations to the larger scale, both in time and space. We use monthly mean current fields from the 1/4° primitive equation model, known as the Parallel Ocean Climate Model (POCM), forced by monthly mean European Centre for Medium-Range Weather Forcasts (ECMWF) winds, which was run for 4 years (April 1986 to December 1989), following the 32-year-long run of the 1/2° model as described by *Semtner and Chervin* [1988,1992]. We will compare its seasonal variability with ship drifts at the surface and with our moored observations. The meridional circulation and heat fluxes of this 1/4° model have been investigated for the Indian Ocean by *Garternicht and Schott* [1997]. Only recently have data from the POCM driven by daily ECMWF winds become available, including the deployment period of the moorings. On the basis of these, we will mainly investigate the behavior of its equatorial jet and Equatorial Undercurrent in comparison to our measurements. Detailed information about the model versions used were given by *Stammer et al.* [1996], who globally compared them with TOPEX/POSEIDON altimetry data and WOCE hydrography with respect to the large-scale circulation. The model variability was found in that study to be low by about a factor of 2 or 4 over a broad spectral range.

2. Observations

An array of six current meter moorings (K4–K9), the second set of moorings within the WOCE ICM8 array, was deployed along 80°30'E (Figure 1) between 45'S and 5°N from July 1993 to September 1994. The moorings were equipped with Aanderaa rotor current meters (RCMs) at several depth levels (Figure 2), and five stations carried upward looking, 150-kHz acoustic Doppler current profilers (ADCPs) at about 180 m depth. The equatorial mooring carried an additional 75-kHz ADCP looking down from just below the upward looking ADCP, yielding high-resolution measurements down to 770 m depth (Plate 1). The northernmost mooring in this second array repeated the position of the central mooring (K2) of the first deployment.

While the measurements from the ADCPs are interpolated to constant depths, the depths of the RCM time

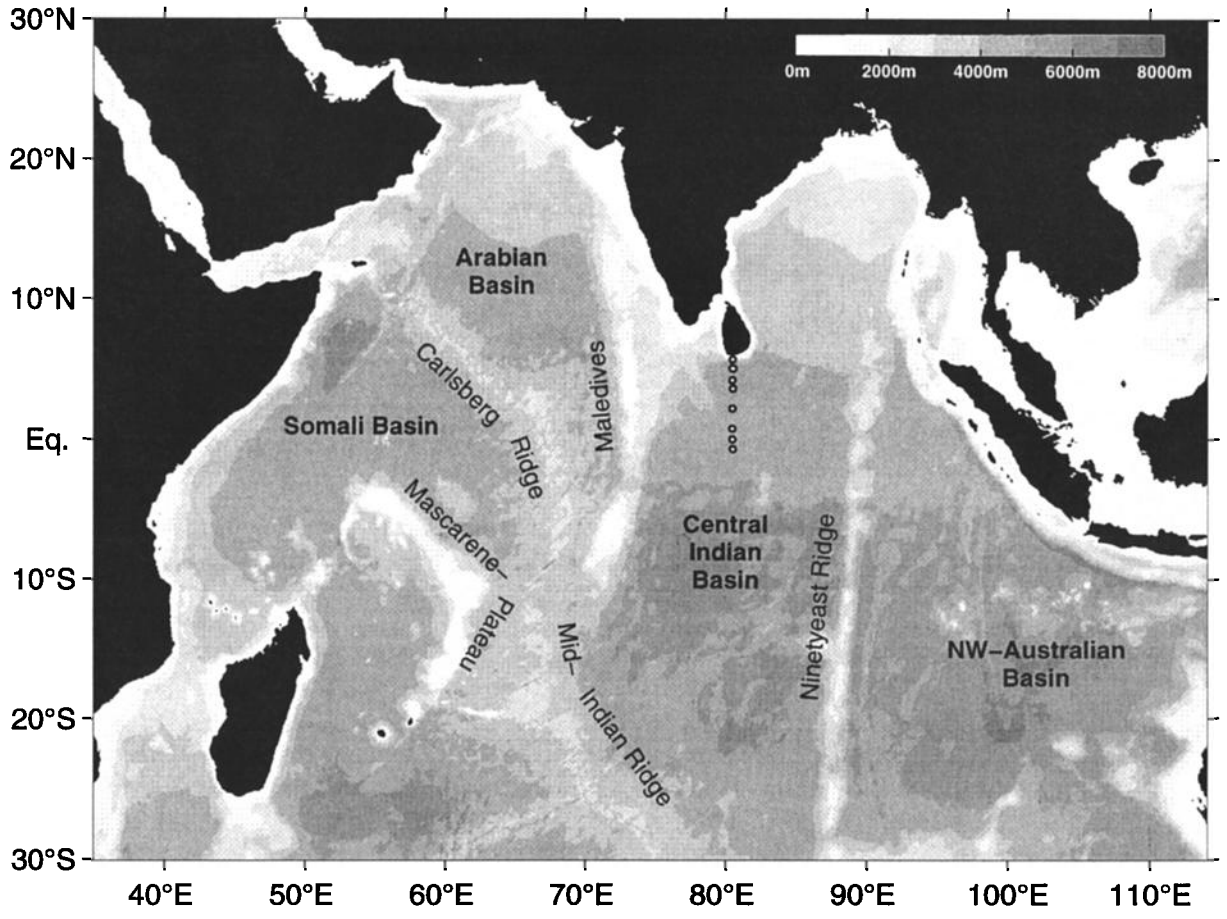

Figure 1. Topography of the Indian Ocean and the positions of moorings K1 to K9 (circles) along 80°30'E south of Sri Lanka.

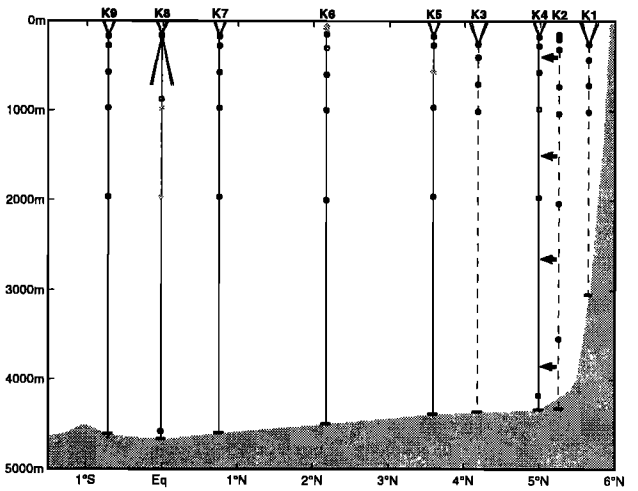

Figure 2. Topography along 80°30'E and current meter distribution on moorings K1 to K9. Solid circles indicate instruments that worked for more than 1 year, stippled circles indicate instruments with shorter time series, and open circles show positions of instruments that did not deliver data. The beams indicate acoustic Doppler current profilers (ADCPs). K1-K3 (dashed lines) were deployed from January 1991 to March 1992, K4-K9 were deployed from July 1993 to September 1994; K4 repeated the position of K2.

series are the mean depths of the instruments. The depths of the ADCPs are calculated from the surface backscatter signals [*Visbeck and Fischer,* 1995]. The level of useful data that was closest to the surface for all ADCPs is the 25-m level; the layer above is contaminated owing to the vertically traveling sidelobe echos from the sea surface.

Vectors of the 40-hour low-passed velocities are shown (rotated 90° anticlockwise) for the two moorings that are representative for the two current regimes, the Monsoon Current and Equatorial Current regime in Figures 3a and 3b, respectively. At the northernmost mooring the surface currents (Figure 3a) are eastward during the deployment of the moorings with values of about 50 cm s^{-1}, while they turn westward in October 1993 with maximum westward values of more than 100 cm s^{-1} in January 1994. The currents change direction again in April 1994 and remain eastward until the recovery of the moorings in September 1994, reaching a second eastward maximum during July/August. This structure can still be seen at 100 m depth but at strongly decreased amplitudes. Below that depth the currents are more variable but have a tendency to be oriented eastnortheastward and westsouthwestward, respectively, which might be due to the currents following the orientation of the continental shelf in that region. An upward phase propagation of the signals is detected, as was discussed in the earlier deployment [*Schott et al.,* 1994].

At the equatorial mooring (Plate 1a and Figure 3b), strong eastward surface currents during September 1993 to January 1994 exceeding 150 cm s^{-1} are the dominant signal. A second period of eastward flow during March until May/June is much weaker (50 cm s^{-1}). This is different from the climatological ship drifts in which the EJ surface currents are smaller in northern fall than spring [*Reverdin,* 1987]. At the 100-m level, however, the eastward flow during February-June is stronger than at the surface, the expression of the EUC. During July-September 1994 an eastward undercurrent appears again on the equator, in contrast to prior knowledge that the EUC only occurs in northern spring. For the deeper levels an upward phase propagation of the currents can be detected.

Annual mean velocities, standard deviations, and fluctuating kinetic energies (FKE) of the 40-hour low-passed time series are presented in Table 1. The statistics are not applied to the whole time series but between August 1, 1993 and July 31, 1994, to avoid a bias by the annual signal. The mean values are mapped in Figure 4. Within the upper 200 m in the equatorial region reaching northward to the mooring at 2°10'N an eastward mean current of more than 22.5 cm s^{-1} exists. At the surface this is due to the dominance of the 1993 fall EJ (Figure 3b), and in the thermocline it is caused by the reoccurrence of the EUC. This annual mean eastward flow is therefore, most likely, not representative of the overall mean near-surface zonal equatorial circulation. The zonal mean component is negative at the deeper equatorial levels, but one does not identify a westward Intermediate Current core in the well-covered ADCP range underneath the EUC, as found in the other oceans. The mean eastward flow within the upper 100 m in the region of the Monsoon Current is in agreement with the findings of the first array and results in a mean westnorthwestward remnant of the NMC in the annual mean. At the equator a change of sign in the mean meridional velocities would take place either if long equatorial Rossby waves of odd meridional modes (those have a zonal current maximum at the equator and the meridional velocities change sign at the equator) are disturbed, e.g., by interannual variability, or when equatorial convergences and divergences would not average out over an annual cycle. The maximum mean meridional currents are located at 0°45'N, where we found the strongest meridional currents.

The FKE decreases fast with depth. The maximum values of more than 1400 cm^2 s^{-2} at the 25-m level at the equator drop to less than 100 cm^2 s^{-2} at the 600-m level. The statistical values at the northernmost station (K4) are similar to those from the first array [*Schott et al.,* 1994]. Mooring K2, which was deployed during 1991-1992 at the position of the present mooring K4, was not equipped with an upward looking ADCP and had its upper RCM at 144 m depth. Annual mean zonal flow at that depth (-6.1±12.6 cm s^{-1}) and meridional velocities (-1.8±9.6 cm s^{-1}) as well as the FKE (125 cm^2 s^{-2}) agree well with the values measured 2

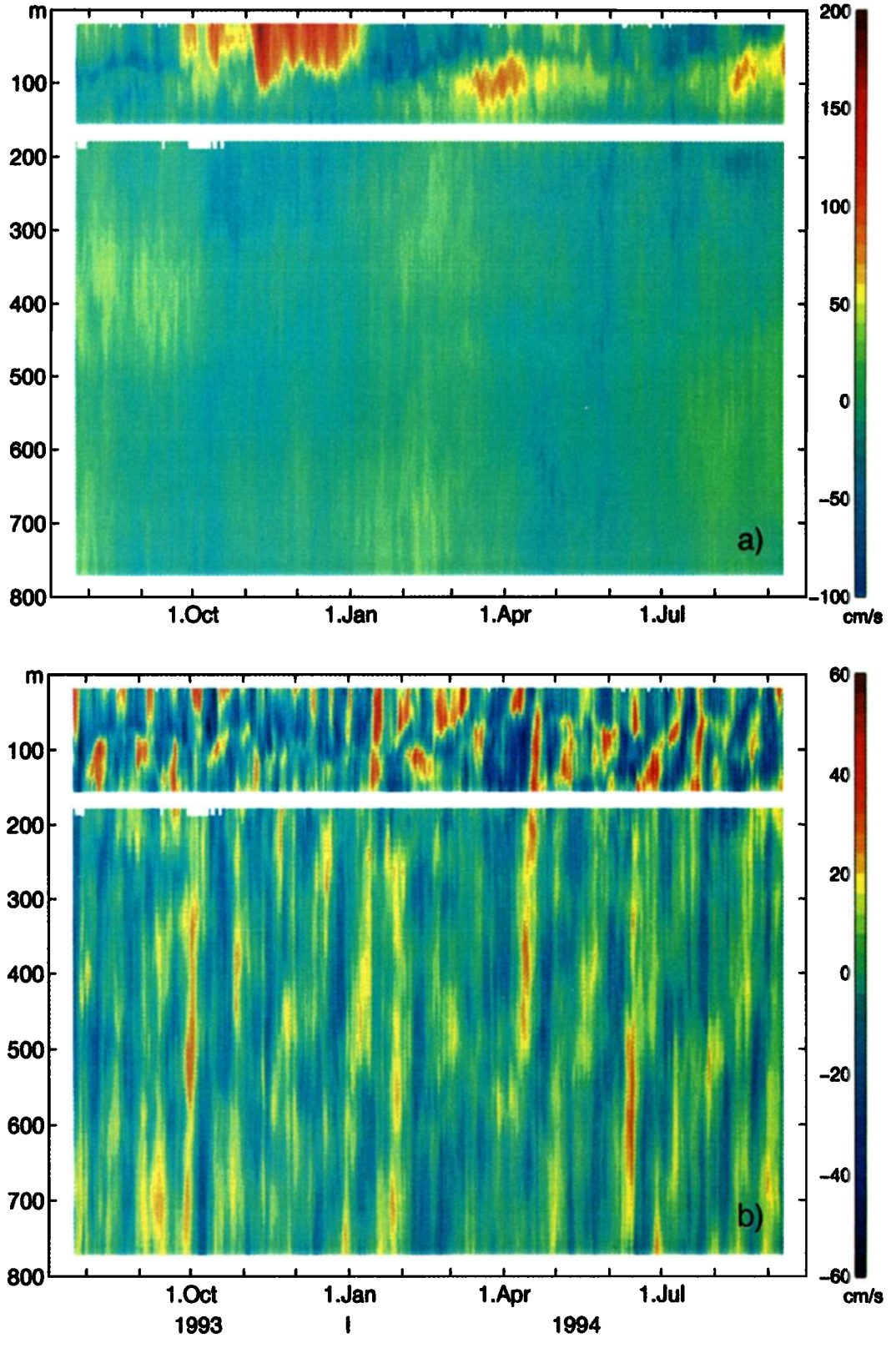

Plate 1. (a) Zonal and (b) meridional 40-hour low-passed velocities at the equatorial mooring as measured by the two ADCPs.

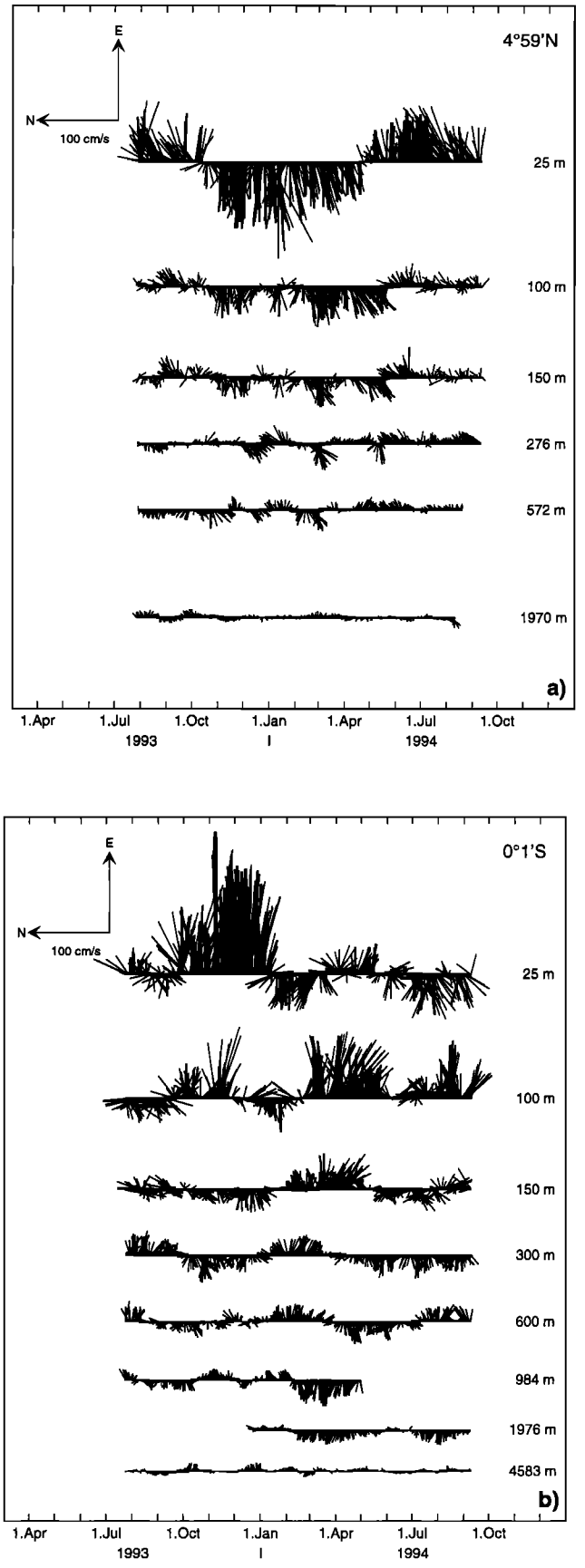

Figure 3. Vector time series of 40-hour low-passed velocities at the (a) northern mooring (K4) and (b) equatorial mooring (K8). Vectors are rotated 90° anticlockwise.

Table 1. Annual Means and Standard Deviations of Current Meter Time Series, August 1, 1993, to July 31, 1994

Record Depth, m	East Component, cm s^{-1}	North Component, cm s^{-1}	FKE*, cm^2 s^{-2}
	Mooring K4, 4°59'N		
25	-7.9 ± 40.6	3.5 ± 16.2	952.6
100	-10.0 ± 16.4	1.3 ± 10.8	193.0
150	-4.5 ± 12.9	-0.3 ± 9.7	129.5
276	-0.0 ± 8.9	-0.4 ± 7.8	69.8
572	-1.6 ± 8.5	-0.2 ± 5.7	52.5
1970	0.5 ± 3.2	0.3 ± 3.4	10.6
	Mooring K5, 3°35'N		
25	-2.5 ± 29.9	5.3 ± 17.3	594.9
100	-9.1 ± 13.4	3.9 ± 11.7	159.0
150	-6.4 ± 12.3	1.8 ± 11.0	135.9
270	-3.2 ± 7.1	1.1 ± 6.2	44.3
567†	1.5 ± 3.1	-0.6 ± 2.6	8.0
963†	-0.9 ± 7.9	1.7 ± 4.5	41.1
1957	1.7 ± 3.8	-0.2 ± 3.1	12.1
	Mooring K6, 2°10'N		
53†	8.3 ± 21.6	4.2 ± 20.2	433.6
93†	8.0 ± 21.0	6.1 ± 12.0	291.7
148†	-1.1 ± 12.3	1.8 ± 10.9	135.8
599	2.3 ± 5.4	-1.7 ± 3.9	22.4
997	1.5 ± 6.2	0.1 ± 5.8	35.7
2001	-2.8 ± 4.1	0.0 ± 3.0	13.0
	Mooring K7, 0°45'N		
25	23.5 ± 44.8	11.5 ± 29.1	1425.0
100	12.9 ± 24.1	3.3 ± 17.3	439.1
150	1.1 ± 13.9	-0.5 ± 12.6	175.4
281	-0.6 ± 14.4	0.7 ± 8.1	136.0
975	-4.0 ± 10.0	1.2 ± 4.8	61.9
1967	1.0 ± 7.8	0.9 ± 4.4	40.3
	Mooring K8, 0°01'S		
25	20.9 ± 50.7	-1.5 ± 17.0	1429.8
100	15.8 ± 26.1	-4.1 ± 17.6	494.7
150	0.3 ± 14.6	-0.7 ± 13.9	202.5
300	-2.3 ± 14.0	-0.7 ± 7.9	129.5
600	-1.4 ± 11.1	-0.2 ± 7.4	88.3
984†	-6.0 ± 11.3	1.3 ± 5.1	77.1
1976†	-6.1 ± 6.1	0.9 ± 4.6	28.8
4583	0.9 ± 3.2	0.0 ± 2.5	8.2
	Mooring K9, 0°43'S		
25	10.1 ± 41.5	-0.3 ± 15.4	979.6
100	10.1 ± 24.0	-4.3 ± 16.7	425.5
150	2.4 ± 13.5	0.1 ± 11.7	158.7
279	-1.3 ± 15.2	-0.9 ± 8.0	146.3
576	0.6 ± 9.2	-0.1 ± 6.4	63.0
973	-5.6 ± 10.0	0.2 ± 6.0	68.3
1965	0.0 ± 5.3	0.5 ± 3.9	21.4

*FKE is fluctuating kinetic energy.
†Short record.

years later at 150 m, while at the deeper levels the FKE is slightly lower during the second deployment.

Variance spectra of the surface currents at the equatorial and the northernmost mooring are shown in Figure 5. The vertical dashed lines mark periods at 365,

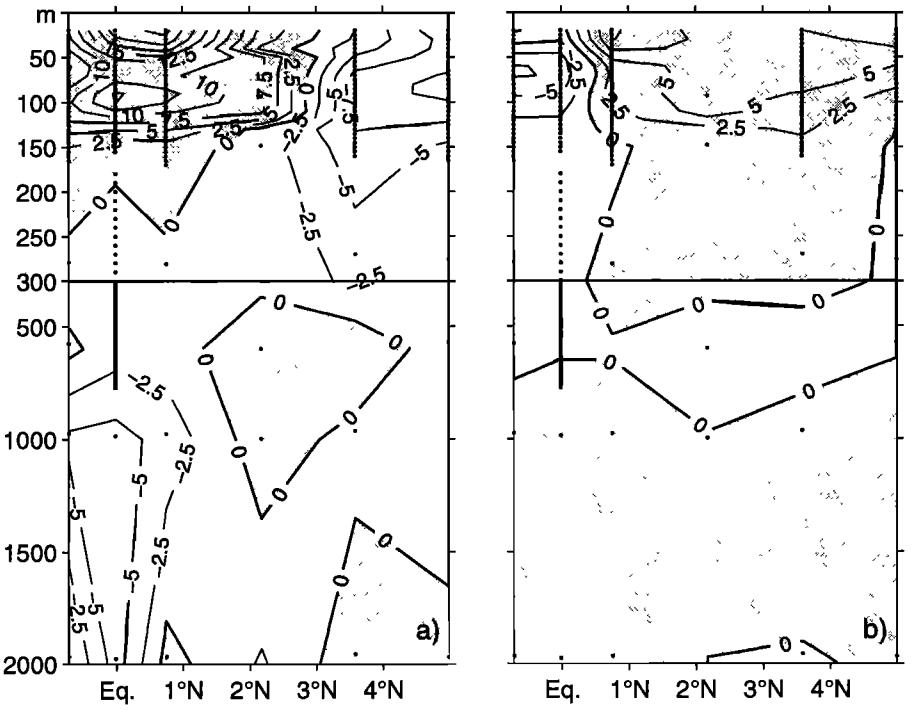

Figure 4. Annual mean (a) zonal and (b) meridional currents between August 1993 and July 1994. The depth scale changes at 300 m.

182.5, and 15.5 days. While the zonal components show maximum variances of 1100 $cm^2\ s^{-2}$ at the semiannual (at the equator) and 400 $cm^2\ s^{-2}$ at the annual (at 5°N) timescale, the meridional components show no energy at these periods. Most of their variance is restricted to the periods of some weeks with a maximum of about 170 $cm^2\ s^{-2}$ at 15.5 days at the equator. In greater depths (not shown) the bands of this intraseasonal fluctuations are spread at distinct periods between 10 and 50 days. That result is in contrast to earlier observations of the equatorial variability in the western Indian Ocean, which found one dominant period of 26 days in the meridional component [*Luyten and Roemmich,* 1982] and sea surface temperature (SST) [*Tsai et al.,* 1992]. Model studies found the source of these 25-to 28-day fluctuation in instabilities of the Southern Gyre at the western boundary [*Kindle and Thompson,* 1989], traveling eastward as Yanai waves.

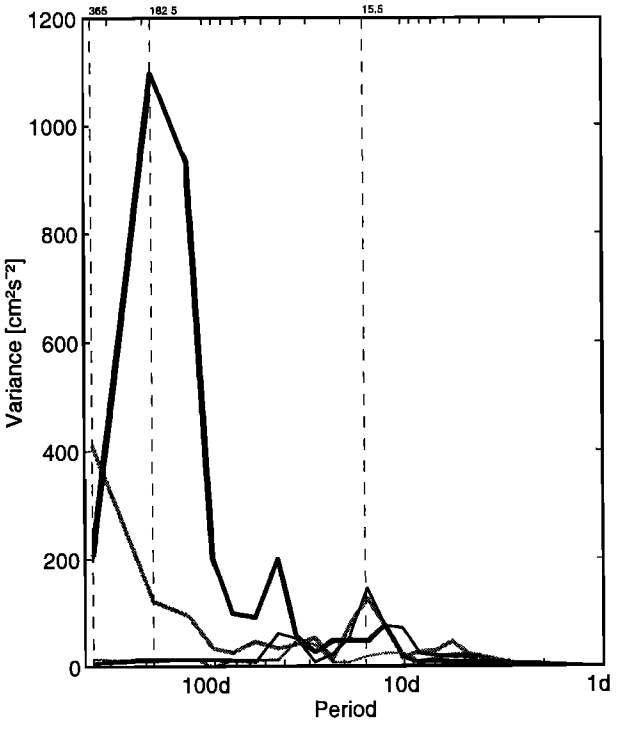

Figure 5. Variance spectra of currents at 25-m depth at the equator (solid lines) and at 5°N (stippled lines) of zonal (thick lines) and meridional (thin lines) components.

The 40-hour low-passed zonal velocities for the upper ocean are shown in Figure 6 for 25-, 100-, 150- and 300-m depth levels in a meridional sequence. Superimposed are the annual and semiannual harmonics that are derived by a least squares fit of the sum of the two harmonics to the low-passed time series for those time series that cover at least 365 days. The amplitudes, phases, and resolved variances are shown in Table 2. One exception is the time series at 3°35'N at 963 m that is just 332 days long. Since the signals with semiannual and annual periods are predominantly zonal, the meridional components are not shown. The zonal component close to the surface at the northernmost mooring is dominated by the annual signal of the Monsoon Current system, while the three moorings around the equator show a comparable semiannual signal in that component. This is in contrast to semiannual components of climatological currents that exceed signifi-

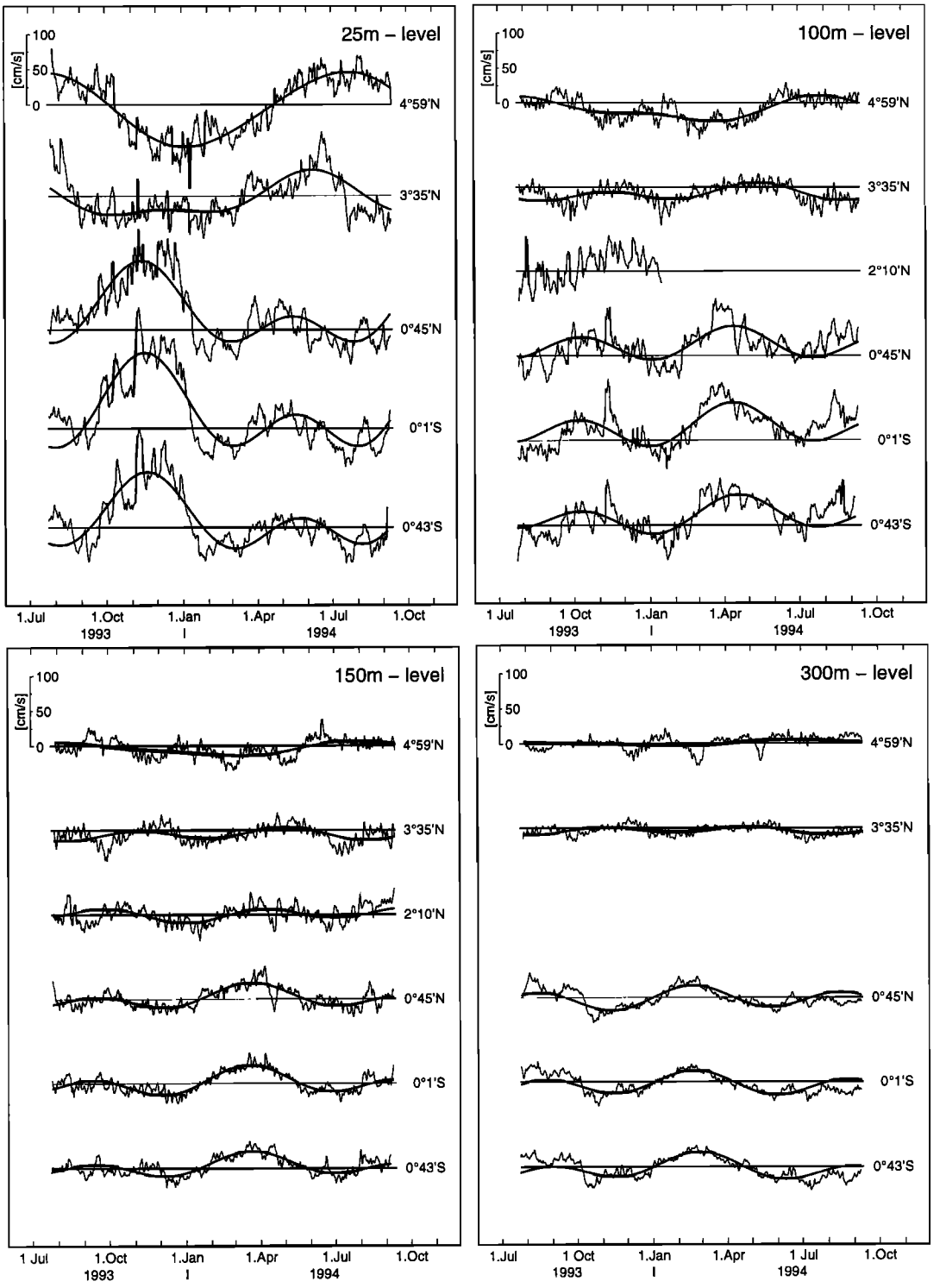

Figure 6. Zonal velocity time series at 25-, 100-, 150-, and 300-m depth. The velocities are 40-hour low-pass filtered, and the thick line superimposed shows the result of the fitted harmonics.

cantly the annual one. The reason for the deviations in our observations is the large spring-to-fall EJ difference 1993/1994 that adds an annual component in the harmonic analysis. The mooring at 3°35'N is influenced by both regimes. While the annual signal close to the coast of Sri Lanka vanishes fast with depth, the semiannual signal around the equator persists through all depths. The first set of moorings had already shown that the Monsoon Currents just reaches down to about 100 m [*Schott et al.*, 1994].

The semiannual harmonics of the zonal currents around the equator show a clear upward phase propagation and thus downward energy propagation (Table 2 and Figure 3b). In 300- to 600-m depth the semian-

Table 2. Amplitudes and Phases of Annual and Semiannual Components in Zonal Currents

Record Depth, m	Annual Amplitude, cm s^{-1}	Annual Phase*, deg	Semiannual Amplitude, cm s^{-1}	Semiannual Phase†, deg	Fraction of Variance Explained
		Mooring K4, 4°59'N			
25	52.4	191	3.4	116	0.83
100	15.0	221	6.5	23	0.55
150	9.4	221	2.5	8	0.33
276	3.8	183	1.3	296	0.09
572	4.8	135	4.8	305	0.31
1970	0.6	353	1.3	140	0.09
		Mooring K5, 3°35'N			
25	28.0	153	12.7	314	0.47
100	6.6	121	8.6	260	0.35
150	3.0	90	7.2	244	0.23
270	1.8	34	4.6	238	0.29
963‡	0.6	328	7.8	135	0.56
1957	0.8	146	3.2	122	0.40
		Mooring K6, 2°10'N			
148	3.4	188	8.1	179	0.22
599	0.6	47	3.3	134	0.19
997	4.1	282	0.1	181	0.20
2001	0.5	197	3.1	304	0.30
		Mooring K7, 0°45'N			
25	40.2	312	34.9	263	0.71
100	7.7	109	19 1	198	0.36
150	10.3	83	11.3	154	0.58
281	5 3	68	13.9	92	0 55
975	3.3	285	10 3	344	0.53
1967	7.6	313	5.0	281	0.65
		Mooring K8, 0°01'S			
25	44.5	316	41.3	270	0.74
100	12.7	114	22.4	195	0.45
150	10.9	86	14.1	146	0.73
300	6.5	38	13.3	102	0.52
600	4.7	343	13.2	66	0.72
4583	1.2	354	0.5	308	0.09
		Mooring K9, 0°43'S			
25	33.1	313	34.5	277	0.69
100	12.5	124	19.1	204	0.42
150	9.3	88	11.5	152	0.59
279	10.3	46	13.1	115	0.54
576	4.1	337	10.0	66	0.61
973	7.1	261	8.1	353	0.52
1965	3.7	301	3.9	293	0.51

*Relative to January 1.
†Relative to January 1 and July 1.
‡Short record (332 days).

nual signal is nearly out of phase with the signal at the 25-m level, with the maxima occurring now in August/September and January/February. At 1000- and 2000-m depth the signal is again about in phase with the surface currents.

The phases of the annual harmonic at 5°N agree with those from the first deployment even at the 2000-m level within the errors, but the amplitude of 0.6 cm s^{-1} is much smaller than during the first deployment (3.9 cm s^{-1}). The explained variances by the annual plus semiannual harmonics generally exceed 50% at the three equatorial moorings. The only exception here is the deepest record right at the equator, where the harmonics explain just 9% of the variance. This time series is the only deep record in the array, and we cannot say whether the low annual and semiannual energy at this

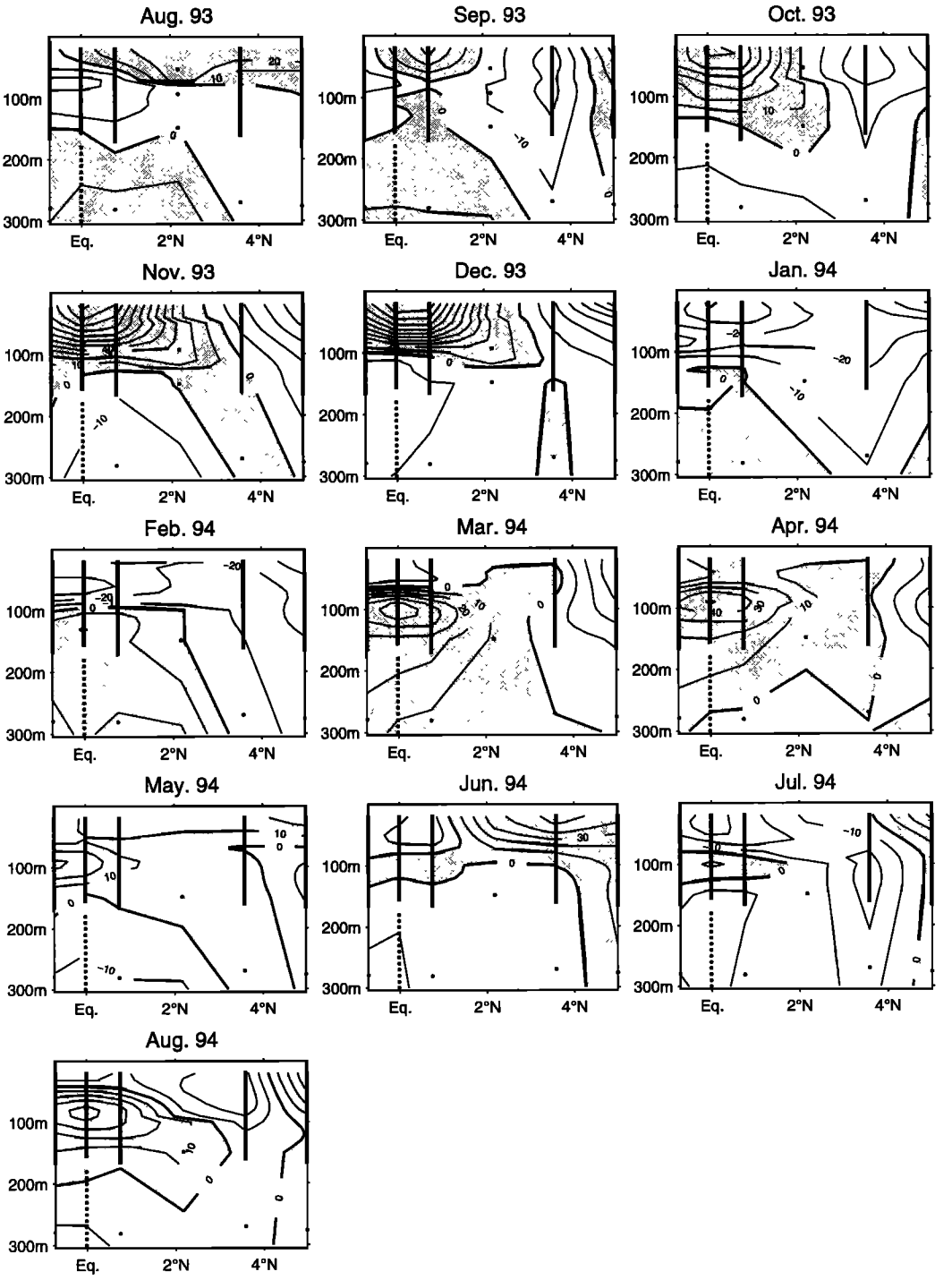

Figure 7. Monthly mean zonal velocities in cm s^{-1} for the upper 300 m. Shaded areas indicate eastward currents.

point is the effect of local topography or whether the energy of annual and semiannual period does not reach these depths in the whole basin. For both the Equatorial and Monsoon Current regime the harmonics explain a large fraction of the variances. Within the surface layer the variance around the equator is explained to about 70%, and in the monsoon current regime, 83% of the surface current variability is explained by the first two harmonics. Here the vertical decay of the explained variance is much stronger than at the equator. In between the two regimes the seasonal cycle explains just about 20 to 40% of the variance.

Only at the 0°45'N mooring do the meridional currents show a quite strong northward signal between about September 1993 and January 1994, which reaches about 60 cm s^{-1} in the fitted semiannual plus annual harmonic and is in phase with those of the zonal currents at this mooring. The other two equatorial

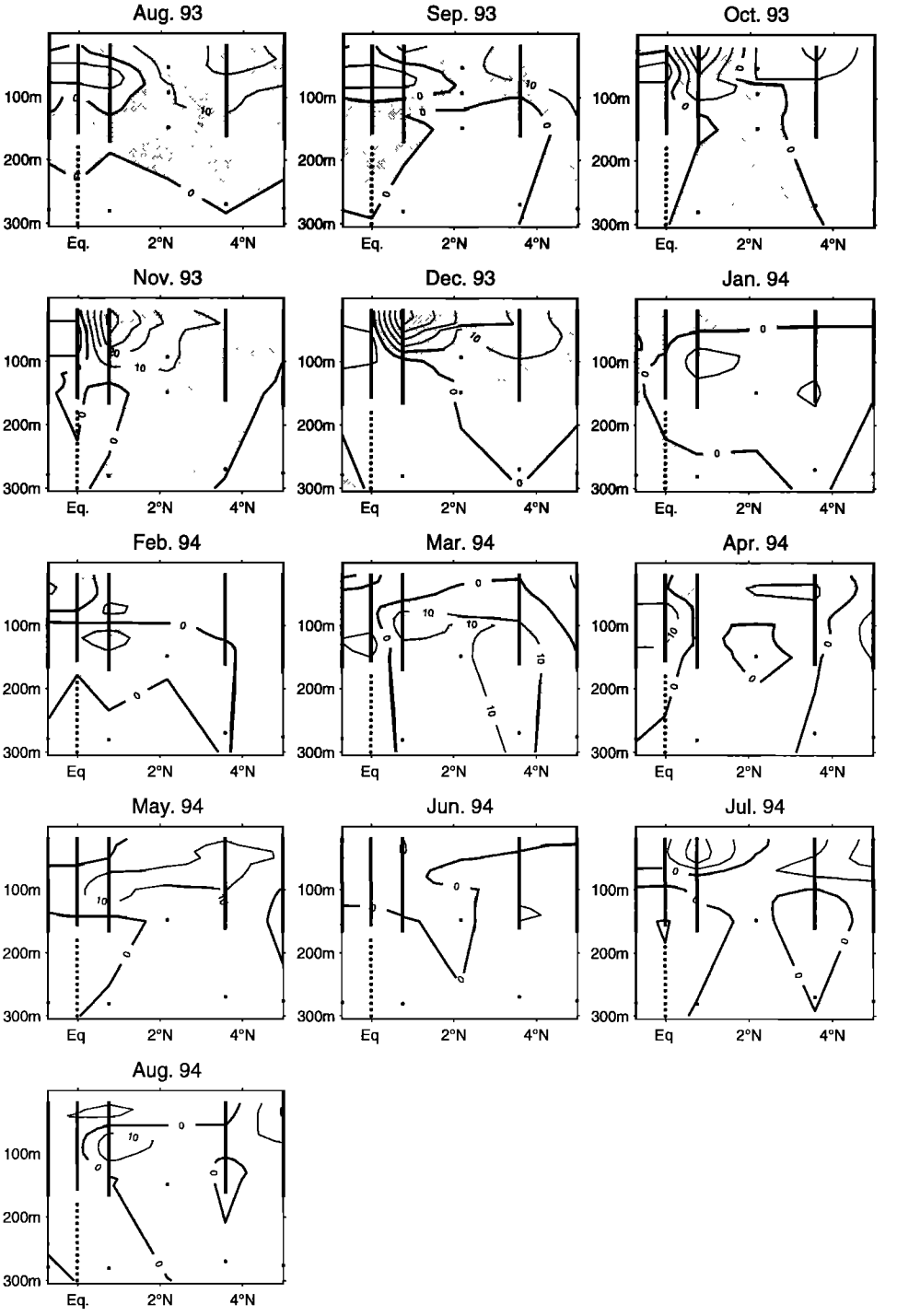

Figure 8. Monthly mean meridional velocities in cm s^{-1} for the upper 300 m. Shaded areas indicate northward currents.

records of meridional velocities are weaker and in opposite phase to the zonal harmonics in the mixed layer.

3. Monthly Means and Transports

To view the currents in a more comprehensive way, monthly mean velocities of both components are mapped onto vertical sections covering the upper 300 m (Figures 7 and 8). In addition, time series of the meridional structure of the flow are produced for 25-m (Figures 9a and 10) and 100-m (Figure 9b) depths. The zonal velocities (Figure 7 and 9) show the eastward SMC confined to the upper 100 m extending southward to the equatorial mooring in August 1993. In September this current is separated into an equatorial current centered at 45'N and the SMC at the northernmost mooring. The equatorial jet increases in strength from about 30 cm s^{-1} in September to more than 110 cm s^{-1} in the monthly

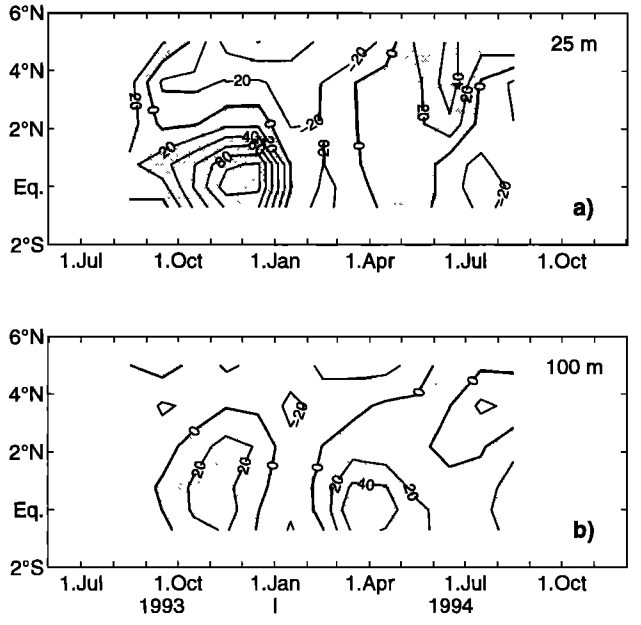

Figure 9. Zonal velocities in cm s^{-1} at (a) 25-m and (b) 100-m depth. Shaded areas indicate eastward currents.

mean of November and more than 100 cm s^{-1} in December 1993 and is centered right at the equator since October. At the two northernmost stations the current reverses in October and the now westward NMC persists until April 1994.

In May the whole area is dominated by an eastward surface current, again, that retracts toward the coast by June. It has to be noted that no measurements exist at 2°N after January 1994 above 150 m. The instruments stopped working because of biofouling. In July and August the limitation of the SMC to the area of the northernmost mooring is evident in the time series of the mooring at 3°35'N.

Along the equator, currents reverse below the eastward surface current. While during the first 2 months another eastward current exists below about 150 m, it disappears during the strong EJ and reappears in January 1994. In February the EUC evolves from this eastward subsurface current and reaches maximum speeds in the monthly mean of more than 50 cm s^{-1} in March

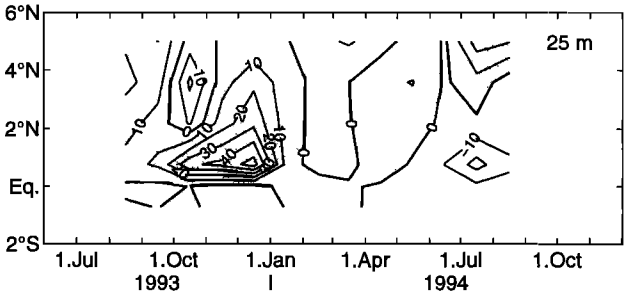

Figure 10. Meridional velocities in cm s^{-1}at 25-m depth. Shaded areas indicate northward currents.

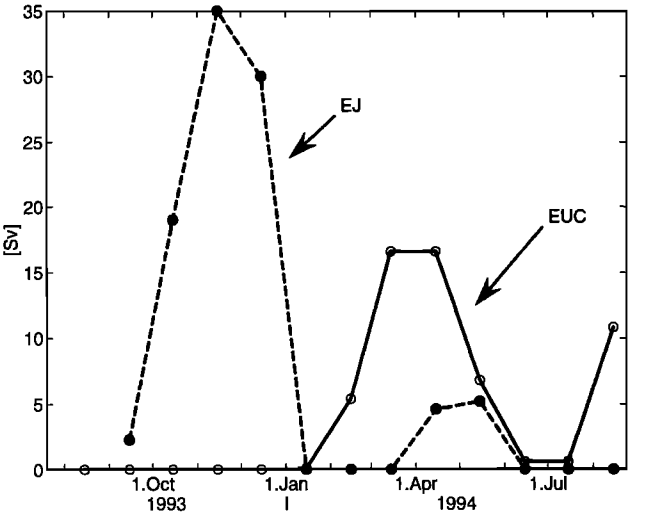

Figure 11. Eastward transport for the equatorial jet (EJ) and the Equatorial Undercurrent (EUC).

1994. The EUC decreases again and is nearly absent in June but reappears again in July and August with a mean speed of more than 40 cm s^{-1}.

The meridional currents (Figures 8 and 10) are generally weaker than the zonal. They also show a vertical structure of reversing currents at the equator. The strongest signal is the northward flow in the upper 100 m at 45'N during the months of October to December 1993 with a maximum value of more than 50 cm s^{-1} in December. It seems to have a slight subsurface maximum at about 35 m depth with values of more than 50 cm s^{-1}.

Monthly mean eastward transports of the EJ and the EUC (Figure 11) based on the flow fields shown in Figure 7 are calculated for the latitude range covered by the array. The shear is linear extrapolated to the surface above 25 m from the two upper depth levels. For the area south of the array the values between 45'N and the northern boundary of the current were doubled to yield an estimate of the total transport. We thereby assume equatorial symmetry of the zonal flow. The velocity patterns at the three equatorial moorings as well as the climatological data (Figure 12) support that assumption. The only exception is the EJ in the September 1993 initial phase that is not symmetric about the equator but is therefore completely covered by the array. The lower boundary for the transport is set to 200-m depth, since sometimes the eastward currents, such as, e.g., the EJ in November 1993, are not confined to one core but extend into the ray-like structures of equatorial waves that continue to greater depths. For May 1994 the transport of the EJ is calculated up to 3°N, about the edge of the EJ in October 1993, as there is no distinct separation between the EJ and the eastward SMC. The transport of the equatorial jet reaches a maximum of 35 Sv in October 1993 but only 4 to 5 Sv in April and May 1994 owing to the low current speeds.

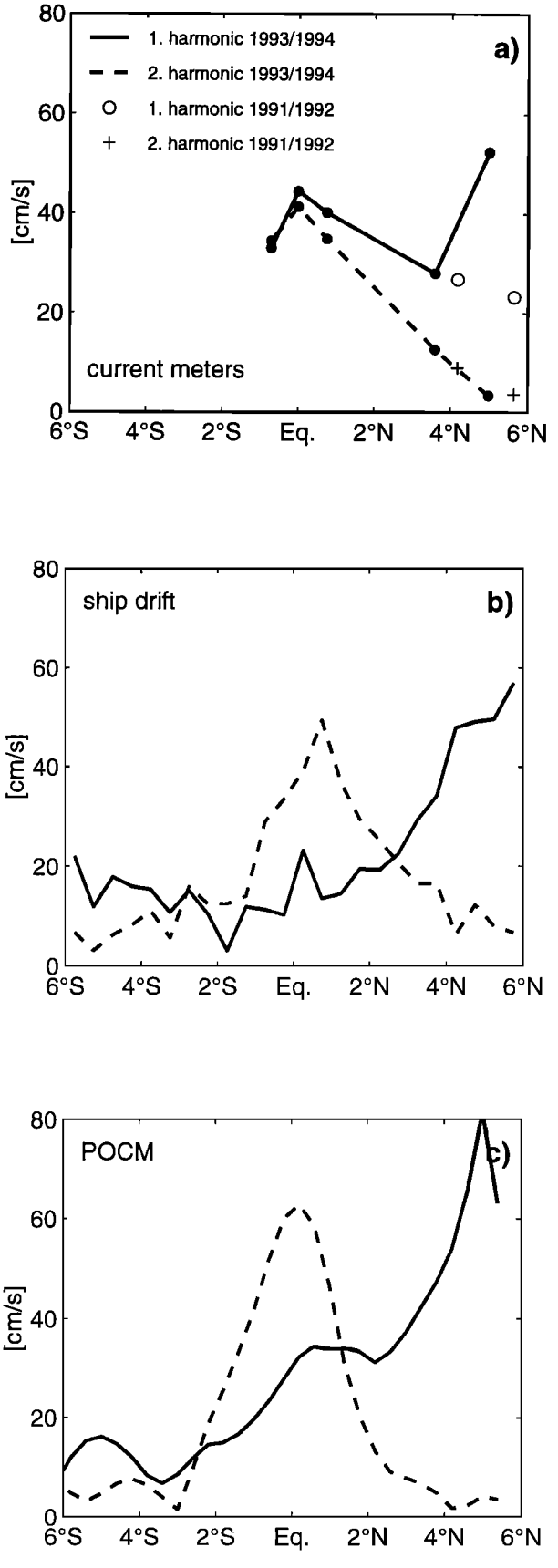

Figure 12. Amplitudes of the first two harmonics fitted to the zonal velocities at the surface for the (a) moorings, (b) ship drifts, and (c) Parallel Ocean Climate Model (POCM).

The Equatorial Undercurrent has its maximum transport of 17 Sv in March and April. It almost disappears during June and July but reappears in August with a transport of 11 Sv. Calculating the transports within a narrow equatorial region, just between 45'S to 45'N, the area of the three equatorial moorings, reveals 8 Sv for the EJ during October 1993 and less than 1 Sv during April/May 1994. The EUC transport within this range reduces to 7 Sv in March and April and 5 Sv in August 1994.

To calculate the transport of the Monsoon Current, we would have to determine it from one mooring (K4) only. The first array had shown that the Monsoon Currents did not remain within one fixed latitudinal band, but rather, meander. We compared the SMC transport at the beginning of our time series with vessel-mounted ADCP measurements during the deployment cruise to see whether it would be reasonable to come up with transports for the Monsoon Current from this array as well. The 7-day mean zonal currents were mapped to a section as the monthly mean values for the equatorial transport calculations. The SMC transport for the first week in August 1993 was 9.7 Sv from the moorings north of 2°N within the upper 300 m. That is just two thirds of the shipboard transport measured on the deployment cruise that was used already in comparison to the transport time series of the Monsoon Current calculated from the data of the first array [*Schott et al.*, 1994]. There are no shipboard transports available from the recovery cruise. Thus the consequence from this comparison is that the second array does not resolve the Monsoon Current well enough to yield transports for it.

4. Discussion

The upper layer equatorial current system in the central Indian Ocean is investigated on the basis of the WOCE current meter array ICM8. Six moorings were deployed along 80°30'E between 45'S and 5°N from late July 1993 to September 1994. This investigation is an extension of the Monsoon Current analysis by *Schott et al.* [1994], who used the first set of moorings (January 1991 to March 1992) north of 4°N and showed the extreme shallowness of about 100 m of the Monsoon Current. The focus of this investigation is on zonal currents and transports of the EJ and EUC. The zonal currents close to the equator have large annual and semiannual contributions, whereas the annual component dominates the upper layer flow at the northern mooring at 5°10'N. The equatorial jet (Wyrtki Jet) in November 1993 is much stronger than the jet in May 1994. The maximum monthly mean transport values for the EJ is 35 Sv in November 1993 and just 5 Sv in May 1994. The Equatorial Undercurrent is apparent during February and June with monthly mean transports up to 17 Sv during March and April. It reappears again in July and persists until the recovery of the moorings in September 1994.

Climatological studies with ship drifts [*Cutler and Swallow,* 1984; *Reverdin,* 1987] show about equally strong EJs with eastward velocities between 60 and 80 cm s^{-1} in the central Indian Ocean. In the eastern basin around our position at 80°E the EJ in spring is with eastward currents of more than 80 cm s^{-1}, slightly stronger than those in fall [*Reverdin,* 1987]. A study of zonal equatorial currents by *Molinari et al.* [1990], derived from satellite-tracked drifting buoys deployed between 1975 and 1987 in the equatorial Indian Ocean, did show the two EJs at both seasons with more than 50 cm s^{-1} about equally strong at 60°E centered at the equator and at 70°E a more intense EJ in fall with more than 75 cm s^{-1}, and the EJ that seems to be centered at about 2°S in spring is less intense with over 50 cm s^{-1}. During that time of the year there are no data available right at the equator at 70°E. Transport calculations from other measurements are scarce. *Donguy and Meyers* [1995] calculated geostrophic transports within the upper 400 m relative to 400 dbar from repeated expendable bathythermograph (XBT) lines in the western Indian Ocean between 1986 and 1989. The easternmost line from Fremantle, Australia, to the Persian Gulf crosses the equator at about 80°E. The transport time series with monthly resolution for the latitudinal bands between 0.5° and 2.5°N (and 0.5-2.5°S) of that line show the semiannual EJs with a pronounced jet during spring. This is in contrast to our measurements, where the jet in fall is much stronger than that in spring, but their observations agree with climatological ship drifts. The transport within the southern part is slightly stronger than in the northern segment. Along the line the peak transports would sum up to 55 Sv for April/May but only 25 Sv for September/October. The order of transports within the EJ compares reasonably with our findings. However, details may differ owing to their choice of a reference level, and the difficulties of the calculation of geostrophic transports close to the equator or may be related to the different period of observations, as interannual variability plays an important role in that area as we will show later.

4.1. Annual Cycle

The seasonal asymmetry of the two jets of this particular year causes an unusual annual harmonic that is in phase with the EJ in fall 1993. To investigate the relationship of our measurements to the climatological annual cycle, we compare our harmonic amplitudes at the surface along the section with those from ship drifts and model data.

The amplitudes of the first and second harmonic of the zonal velocities at 25 m depth are shown in Figure 12a. The values from the first array are included in the graph for comparison. Both harmonics show a maximum at the equatorial mooring and fall off to both sides. Both are in phase across the equator (Table 2). While the amplitude of the second harmonic decreases to near zero close to the coast, the first harmonic reaches its maximum with 52.4 cm s^{-1} at the northernmost mooring. Whereas the amplitudes of the second harmonic agree very well with those from the first deployment, the coastal value of the first harmonic is much higher than the values from the first deployment. There were no data at that depth at the center position of the first array, but the data at 150- and 200-m depth during the first deployment period [*Schott et al.,* 1994] also revealed a maximum for both amplitudes at the central position and a decay toward the coast.

The individual ship drift observations from *Cutler and Swallow* [1984] are averaged to climatological monthly means along the section between 79° and 82°E with 0.5° latitudinal resolution. The harmonics from the POCM data are calculated from the time series of monthly means for April 1986 to December 1989. The most striking difference between our observations (Figure 12a) on the one hand and ship drifts (Figure 12b) and the POCM (Figure 12c) on the other hand is the equatorial peak of the first harmonic in the observations, which is caused by the different amplitudes of the two equatorial jets in fall 1993 and spring 1994. The semiannual signal in the ship drifts of 50 cm s^{-1} is slightly stronger than that in the current measurements and is slightly shifted to the north at 1°N. This could be an effect of the long averaging intervals on the ship data, as many shipping lanes turn to the north after passing the southern tip of the Indian subcontinent. These data have been calculated for latitude ranges farther south than the extent of the array. They show that the semiannual harmonic is symmetric about the equator, while the annual harmonic is intensified toward the coast. The amplitudes of the harmonics in the model are generally higher than those of the current measurements and ship drifts, but the structure agrees well with the ship drifts. Here the peak for the semiannual harmonic is centered at the equator and the first harmonic shows a maximum at 5°N and decreases again toward the coast, supporting the measurements.

As shown by *Cane* [1980] the existence of the EUC in the Indian Ocean is related to easterly winds, forcing a westward surface current that builds up the pressure gradient to maintain the eastward undercurrent. Interpreting the measurements at Gan (0.5°S, 73°E) by *Knox* [1976], *Cane,* [1980] suggested that the strength of the wind forcing during the last quarter of the previous year influences the strength of the EUC in the following year owing to a reflection of equatorial waves at the eastern boundary. In 1972 the winds remained weak from October through December followed by an EUC in spring, while in 1973 there were strong westerlies throughout this period but no EUC in spring. This does not fit with our observations, as we have a very strong eastward wind anomaly during the EJ in late 1993 and still find the EUC in the following spring. The EUC in spring 1994 and its reappearance seem to

be forced by westward winds in the same year. The FSU pseudo wind stresses [*Legler et al.*, 1989] along the equator show an onset of westward winds at the western boundary in September and October 1993 (Figure 13a). The regime of westward winds reaches the central basin in January 1994. As a consequence, the eastward EJ in the central Indian Ocean is decelerated in December and January (Figure 9a) and the surface currents turn westward in January. The EUC appears at 80°E in February (Figure 9b) with some delay to the wind-forcing as to be expected [*Cane*, 1980] since the zonal pressure gradient needs to be built up to force the undercurrent. The onset of eastward winds in the western basin during April and May 1994 and the induced eastward surface jet that we see at 80°E during these two months then seem to decrease the zonal pressure gradient and decelerate the EUC (Figure 9b). The eastward winds and the EJ are anomalously weak in spring 1994 (Figure 13b), as we will show later, and as a result, the zonal pressure gradient is probably not completely eroded. The onset of the westward winds in the eastern parts of the ocean during May and June 1994 and the resulting westward surface currents increased the pressure gradient and thus the eastward undercurrent again. A model study using a general circulation model of the Indian Ocean driven by two different wind fields (ECMWF and United Kingdom Meteorological Office (UKMO)) by *Anderson and Carrington* [1993] showed a second undercurrent that was in contrast to the measurements available at that time.

The seasonal cycles of meridional currents in our observations are in phase with those of the zonal currents in the mixed layer at 0°45'N and of opposite phase at the two southern moorings (Figure 9 and 10). We observe a divergence during the EJ from September until December 1993 in the upper 100 m and a convergence during situations with westward surface currents (February/March 1994 and June to August 1994). Following *Cane* [1980], eastward winds would force an equatorial convergence at the surface and a divergence below the thermocline. Westward winds would force a westward surface current, a surface divergence, and a convergence below. This is in contrast to our measurements. The meridional signal of long equatorial Rossby waves could not account for that signal, as their meridional currents are 90° out of phase with the zonal currents.

4.2. Interannual Variability

Is the strong difference of the two observed equatorial jets the result of larger-scale interannual variability? *Anderson and Carrington* [1993] have shown with their general circulation model of the Indian Ocean driven by the two different wind fields that the currents exhibit strong diffences between the two forcing fields as well as strong interannual variability. In both cases the equatorial region is the area of the Indian Ocean with the strongest differences. As our time series alone are too short to answer this question, the ship drift data from *Cutler and Swallow* [1984] are used to investigate the interannual differences in the strength of the EJ. The zonal component of the individual observations are averaged for every month from 1970 to 1982 for the central Indian Ocean within the box 60-90°E and ±1° latitude. The mean annual cycle of the drifts shows nearly equally strong jets of about 50 cm s^{-1} in spring and fall. The mean annual cycle for the upper layer in the POCM driven by monthly winds for the same geographical domain is somewhat different at 75 cm s^{-1} in fall and 90 cm s^{-1} in spring. This is probably due to the shortness of the interval (1986-1989) studied with the POCM.

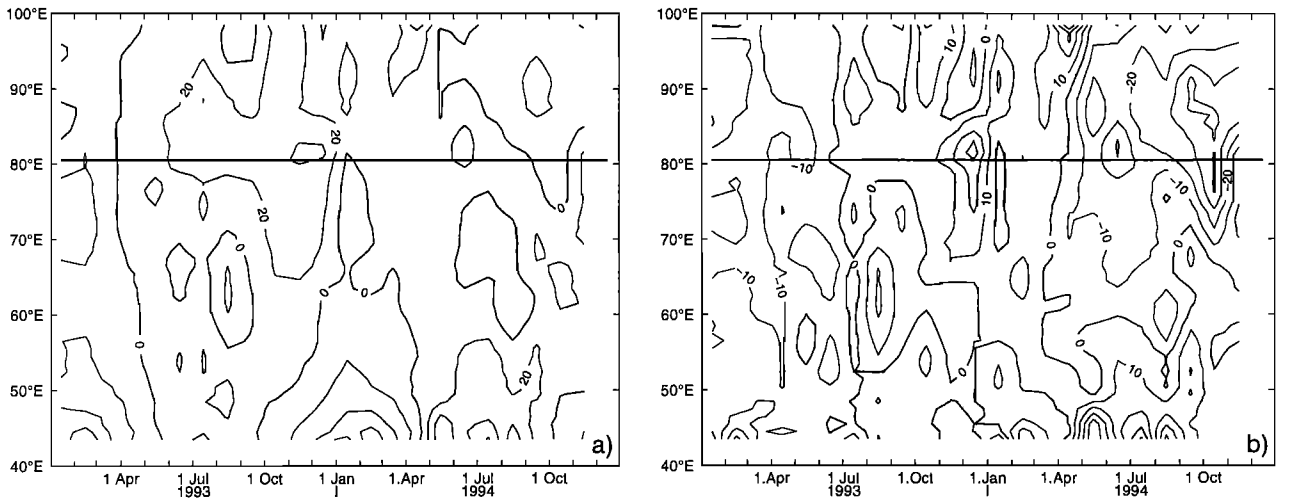

Figure 13. (a) Zonal Florida State University (FSU) pseudo wind stress (eastward is shaded) along the equator and (b) its anomaly relative to a mean annual cycle for 1970 to 1993. The horizontal line indicates the position of the mooring line at 80°30'E.

The anomaly of the zonal ship drifts from their mean annual cycle for the years 1970 to 1982 (Figure 14b) shows that there is indeed an interannual signal, which is not only restricted to the periods of the EJs but also affects the total zonal transport throughout the years. The same anomaly is computed for the model data by subtracting their mean annual cycle and for the average zonal velocities from the three equatorial ADCPs at 25-m depth. Owing to the lack of a mean annual cycle of the latter, the mean annual cycle of the ship drifts is used as a reference (Figure 14b).

In a comparison of the zonal ship drift velocity anomaly with the Southern Oscillation Index (SOI), the pressure difference between Tahiti and Darwin (Figure 14a) shows some remarkable similarities of certain anomalies. The anomaly of the zonal pseudostress for the same region (Figure 14c) shows a similar interannual signal. Although the time series are not significantly correlated, all three time series reflect the El Niño (low SOI) of 1971/1972, 1982/1983, 1986/1987, 1992/1993, and 1993/1994 and the intermediate La Niña periods. During the El Niño conditions the zonal wind stress and zonal currents are weaker, whereas they tend to be stronger during the high SOI periods.

The shorter time series for the deployment time of the moorings for the wind stress anomaly, the SOI and the anomaly of the zonal currents derived from the ADCP data, and the mean annual cycle of the ship drifts (Figure 15) are all correlated with each other within the 95% level of significance even at a relative small number of degrees of freedom (4). The autocorrelation functions of all three time series show the zero crossings after 3 months. The correlation coefficients are $r = 0.92$ for the current anomaly versus the wind stress anomaly, $r = 0.85$ for the correlation between the current anomaly and the SOI, and $r = 0.72$ for the correlation between the wind stress anomaly and the SOI. Both, the maximum and minimum of the zonal anomalies coincide with one of the EJs during the deployment, resulting in the very strong jet in November 1993 and the much weaker jet in May 1994. Thus the difference between the amplitudes of these two jets is related to the ENSO phenomenon.

A study about the zonal equatorial wind stress by *Clarke and Lebedev* [1997] showed no correlation between the interannual zonal wind stress in the Indian and Pacific Oceans for the complete period covered (1950-1992). The zonal wind stress in the Indian Ocean and that in the Pacific are found to be negatively correlated for the later period 1970-1992 which is close to our observations. *Meyers* [1996] showed that the Indonesian throughflow is correlated with the SOI and

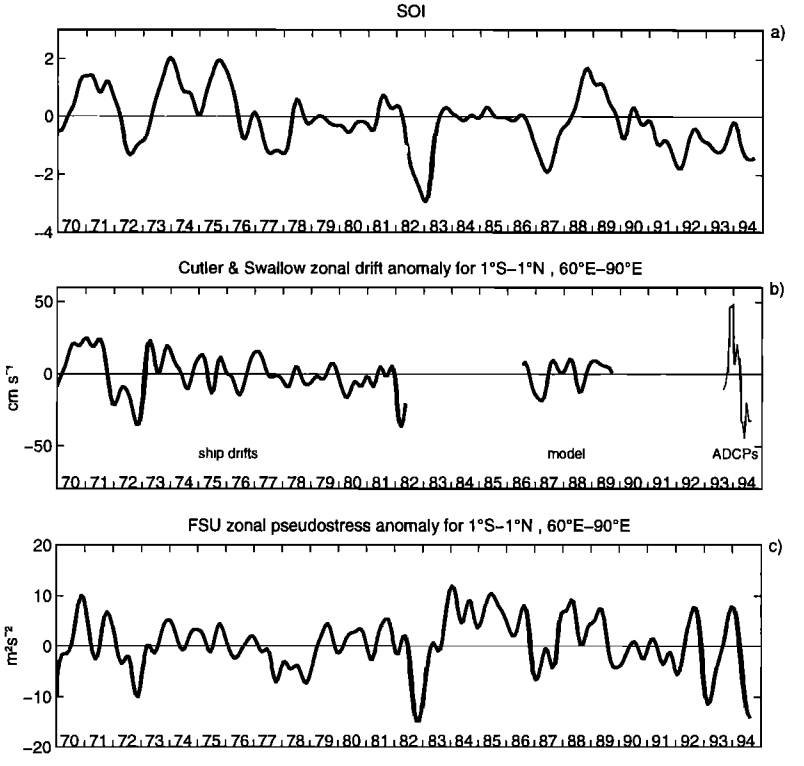

Figure 14. Six-month low-passed time series of monthly mean values of (a) the Southern Oscillation Index (SOI), (b) the anomaly of zonal ship drift (until 1982), and the mean zonal current of the three equatorial ADCPs (unfiltered) at 25-m depth, both referenced with the mean annual cycle of the ship drifts and the zonal anomaly of the model currents (1986-1989) from their mean annual cycle. (c) Anomaly of the zonal FSU pseudostress within the same geographical domain.

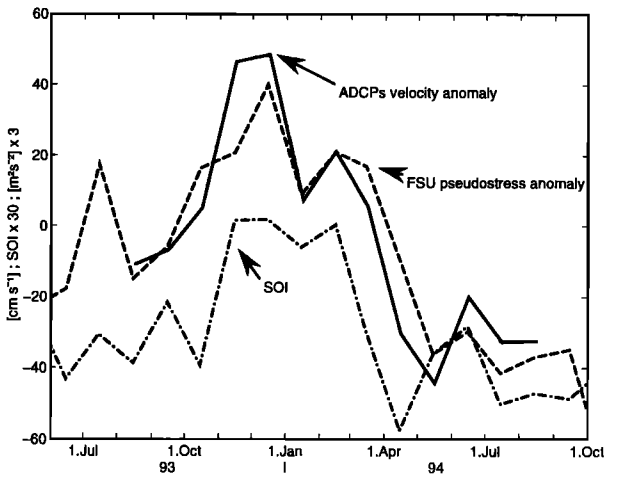

Figure 15. Monthly mean values for the anomalies of the zonal surface currents at the three equatorial moorings and the anomalies of the zonal FSU pseudostress and the SOI.

that the origin of that signal should be in the equatorial Indian Ocean as well as in the Pacific. He used a repeated XBT section between Java and western Australia from 1983 to 1994. The transport of 1988-1989 was about 5 Sv higher than during the preceding and following ENSOs. He suggested that these variabilities in the equatorial Indian Ocean propagated along the eastern boundary as *Clarke and Liu* [1994] showed for interannual fluctuations in sea level.

4.3. Model Comparison

In order to relate our observations to the basin scale equatorial circulation, we analyze monthly mean currents from the POCM-4b driven by daily ECMWF winds. The zonal surface currents simulated by the model show two jets of different strength along the equator (Figure 16a). While the EJ during late 1993 reaches maximum eastward speeds of more than 140 cm s^{-1}, the EJ during early 1994 just exceeded 60 cm s^{-1}. These differences exist mainly west of the Maledives (at about 73°E). The model currents do not resemble our measurements along 80°E (Figures 16b and 9a), where the model jet in fall 1993 is less than 80 cm s^{-1} while peak values of more than 60 cm s^{-1} are obtained for April 1994. The most likely reason for this behavior is that the Maledives represent a barrier in the model that is too restrictive and the jet is meandering east of the islands (Figure 16b). The harmonics for the upper layer along the section for this model version (Figure 17) compared to the previous run (Figure 12c) result in lower amplitudes for the second harmonic (40 cm s^{-1} at the equator) that agree reasonably with the moored measurements, but it now shows secondary maxima at 4°N and 4°S and an increase toward the coast to amplitudes of 22 cm s^{-1} that are not observed. As expected, the annual harmonic does not show the equatorial maximum at 80°E seen in the measurements, while it agrees with the measurements of the coastal structure of the Monsoon Current system, as it reveals a maximum of about 60 cm s^{-1} at 4°N and and a decay to values of less than 40 cm s^{-1} directly at the coast.

Sections of the zonal velocities (cm s^{-1}) along 80.6°E for the upper 300 m (Figure 18) for November 1993 and April and August 1994, the months of maximum transports of the EJ and EUC in the current measurements,

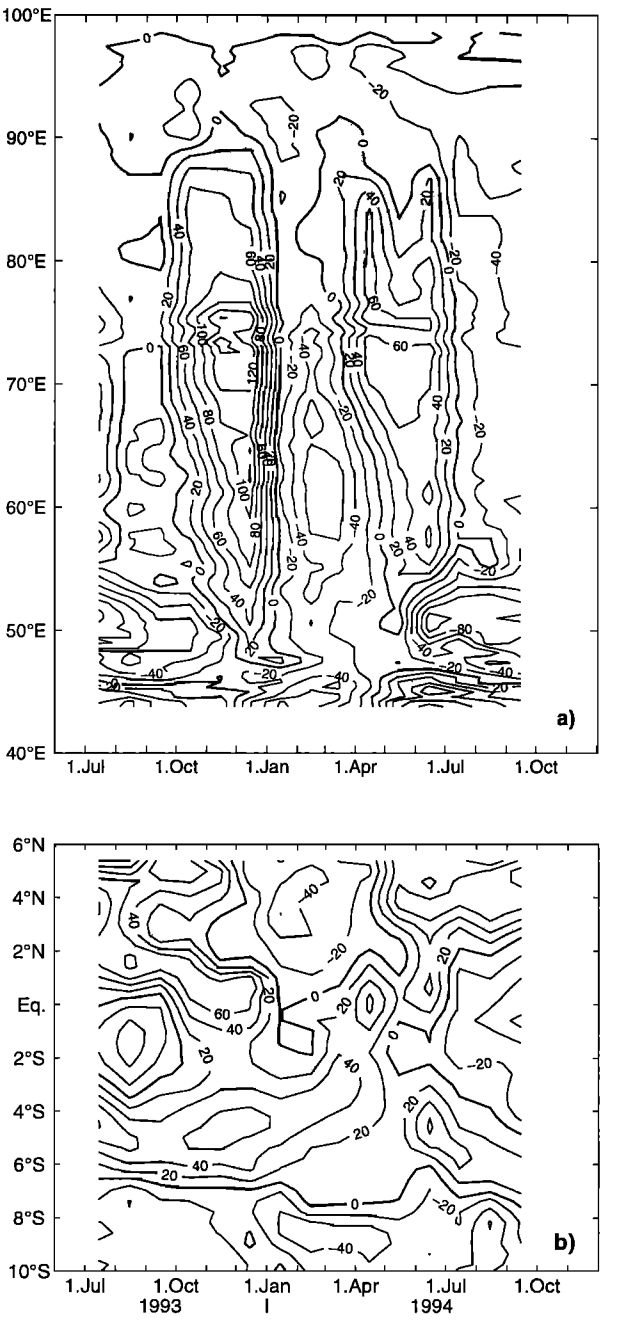

Figure 16. Zonal currents in the upper model layer from the POCM driven by daily winds for the deployment period (a) along the equator and (b) along 80.6°E.

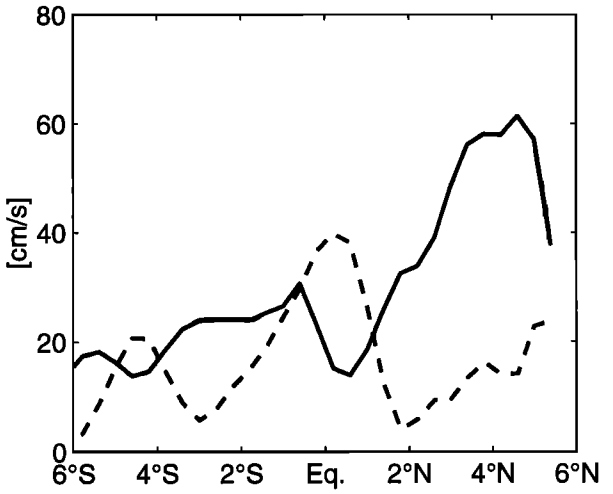

Figure 17. Amplitudes of the first two harmonics fitted to the zonal velocities at the surface as in Figure 12c, but for the POCM model driven by daily winds.

compare generally well with the current structure derived from our measurements (Figure 7). As seen in the surface currents along the section (Figure 16b), the EJ in November 1993 is not strong enough in the model. During November the current meter measurements at 3°35'N and 5°N show the westward NMC while the model still shows an eastward SMC north of the westward current between about 2° and 3°N. In April 1994 the EJ in the model is much too strong, as discussed before. The NMC in the model has a strength and width comparable to the measurements. The westward current south of the Monsoon Current might not be resolved by our array. The undercurrent forming is weaker than in our observations. It has two off-equatorial maxima in the model during April and August but just one equatorial maximum during December 1993 to March 1994. During August 1994 the SMC is again too strong and reaching too far south. The model does not show an EUC along the equator through the whole basin, as is known from the other oceans. Along 80.6°E the model produces an eastward undercurrent that has its core within the layer between 100 and 135 m. It is apparent from December 1993 to August 1994 but not during July and August 1993. What appears to be the EUC during spring is fed by an undercurrent south of the equator from the western basin (Figure 19a). Observations of the undercurrent in the Indian Ocean have shown the EUC slightly south of the equator, centered at 1° to 1.5°S [*Leetmaa and Stommel,* 1980] in the western basin but not that far south. The model undercurrent in the eastern basin is connected as well to an eastward undercurrent at that time, which has a much deeper equatorial core in the western basin around 400- to 500-m depth and is obviously related to equatorial waves. Both undercurrents vanish in the western basin during June, but east of the Maledives the undercurrent persists (Figure 19b). This coincides with the westward winds being limited to the eastern basin during that time.

It is not clear exactly how these undercurrents are forced and whether they are the product of the EUC forcing mechanisms described by *Cane* [1980]. Furthermore, it is not clear how well the EUC in the Indian Ocean is modeled by the POCM as the coarse vertical

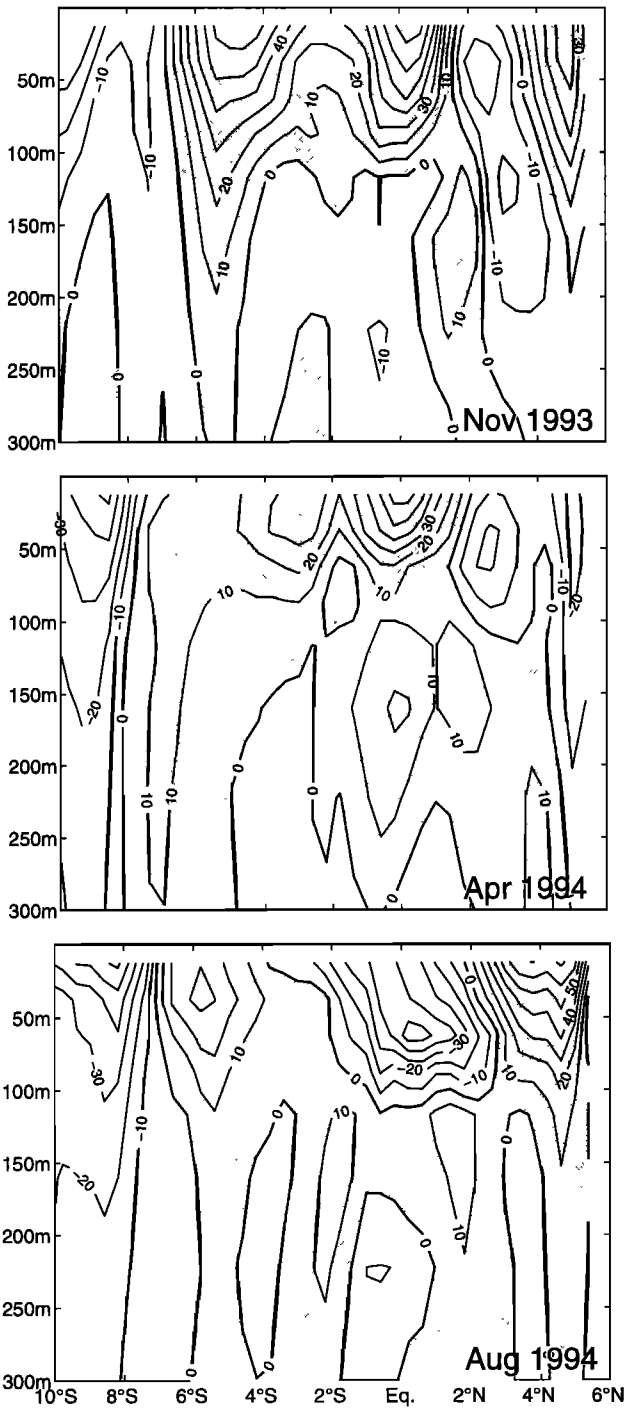

Figure 18. Monthly mean zonal currents for November 1993, April 1994, and August 1994 along 80.6°E from the POCM driven by daily winds. Contour interval is 10 cm s^{-1}. Shaded areas indicate eastward currents.

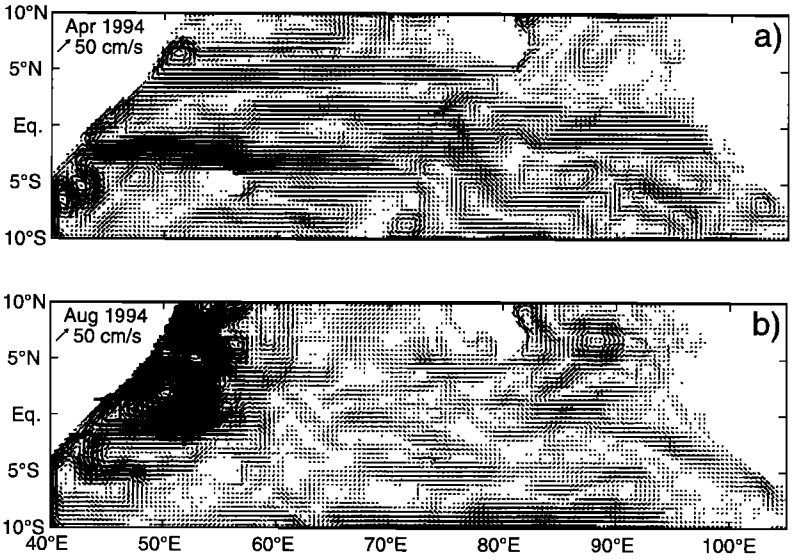

Figure 19. Current vectors from the POCM driven by daily winds for the level between 100 and 135 m for (a) April 1994 and (b) August 1994.

resolution (with a minimum layer thickness of 25 m in the upper four layers) might limit its ability to properly reproduce the EUC. With regard to the discrepancies between the model and our measurements it seems unclear whether the origin of the EUC observed in our measurements at 80°E is that shown in the model and needs further investigation.

In addition to the POCM a 3.5-layer reduced gravity Indian Ocean model forced by either 12-hourly ECMWF wind stresses or by FNMOC 12 wind stresses was inspected and showed interannual variability of the zonal currents within the upper two layers, which include the EJ and EUC. In contrast to the POCM data, this model shows no blocking of the equatorial jets by the Maledives but strong differences, depending on the wind field used (J. Kindle, personal communication, 1998).

Acknowledgments. We would like to thank the captains and crews of the R/V *Sonne* and R/V *Franklin* for their help during the deployment and recovery of the moorings. We thank A. Semtner and R. Tokmakian for making the POCM model data available and J. Kindle for evaluating his model for us. Funding was obtained by the German WOCE program through BMBF grants 03F0121A and 03G0088A.

References

Anderson, D. L. T., and D. J. Carrington, Modeling interannual variability in the Indian Ocean using momentum fluxes from the operational wheather analyses of the United Kingdom Meteorological Office and the European Centre for Medium Range Weather Forecasts, *J. Geophys. Res.*, *98*(C7), 12,483–12,499, 1993.

Cane, M. A., On the dynamics of equatorial currents, with application to the Indian Ocean, *Deep Sea Res., Part A*, *27*, 525–544, 1980.

Clarke, A. J., and A. Lebedev, Interannual and decadal changes in equatorial wind stress in the Atlantic, Indian, and Pacific Oceans and the eastern ocean coastal response, *J. Clim.*, *10*, 1722–1729, 1997.

Clarke, A. J., and X. Liu, Interannual sea level in the northern and eastern Indian Ocean, *J. Phys. Oceanogr.*, *24*, 1224–1235, 1994.

Cutler, A. N., and J C. Swallow, *Surface currents of the Indian Ocean (to 25° S, 100° E)*, Inst. of Oceanogr. Sci., Wormley, England, 1984

Donguy, J R., and G. Meyers, Observations of geostrophic transport variability in the western tropical Indian Ocean, *Deep Sea Res., Part I*, *42*, 1007–1028, 1995.

Düing, W., and F. Schott, Measurements in the source region of the Somali Current during the monsoon reversal, *J. Phys. Oceanogr.*, *8*, 278–289, 1978

Fischer, J., F. Schott, and L. Stramma, Currents and transports of the Great Whirl - Socotra Gyre system during the summer monsoon, August 1993, *J. Geophys. Res.*, *101*(C2), 3573–3587, 1996.

Garternicht, U., and F. Schott, Heat fluxes of the Indian Ocean from a global eddy-resolving model, *J. Geophys. Res.*, *102*(C9), 21,147–21,159, 1997.

Kindle, J. C., and J. D. Thompson, The 26- and 50-day oscillations in the western Indian Ocean: Model results, *J. Geophys. Res.*, *94*(C4), 4721–4736, 1989.

Knox, R. A., On a long series of Indian Ocean equatorial currents near Addu atoll, *Deep Sea Res., Part A*, *23*, 211–221, 1976.

Leetmaa, A., and H. Stommel, Equatorial current observations in the western Indian Ocean in 1975 and 1976, *J. Phys. Oceanogr.*, *10*, 258–269, 1980.

Legler, D. M., I. M. Navon, and J. J. O'Brien, Objective analysis of pseudostress over the Indian Ocean using a direct-minimization approach, *Mon. Weather Rev.*, *117*, 709–720, 1989.

Luyten, J. R., and D. H. Roemmich, Equatorial currents at semi-annual period in the Indian Ocean, *J. Phys. Oceanogr.*, *12*, 406–413, 1982.

McCreary, J. P., P. K. Kundu, and R. L. Molinari, A numerical investigation of dynamics, thermodynamics

and mixed-layer processes in the Indian Ocean, *Prog. Oceanogr.*, *31*, 181–244, 1993.

Meyers, G., Variation of Indonesian throughflow and the El Niño-Southern Oscillation, *J. Geophys. Res.*, *101*(C5), 12,255–12,263, 1996.

Molinari, R. L., D. Olson, and G. Reverdin, Surface current distribution in the tropical Indian Ocean derived from compilations of surface buoy trajectories, *J. Geophys. Res.*, *95*(C5), 7217–7238, 1990.

Rao, R. R., R. L. Molinari, and J. F. Festa, Evolution of the climatological near-surface thermal structure of the tropical Indian Ocean, 1, Description of mean monthly mixed layer depth, and sea surface temperature, surface current, and surface meteorological fields, *J. Geophys. Res.*, *94*(C8), 10,801–10,815, 1989.

Reverdin, G., The upper equatorial Indian Ocean: The climatological cycle, *J. Phys. Oceanogr.*, *17*, 903–927, 1987.

Schott, F., J. C. Swallow, and M. Fieux, The Somali Current at the equator: Annual cycle and transports in the upper 1000 m and the connection to neighbouring latitudes, *Deep Sea Res., Part A*, *37*, 1825–1848, 1990.

Schott, F., J. Reppin, J. Fischer, and D. Quadfasel, Currents and transports of the Monsoon Current south of Sri Lanka, *J. Geophys. Res.*, *99*(C12), 25,127–25,141, 1994.

Schott, F., J. Fischer, U. Garternicht, and D. Quadfasel, Summer monsoon response of the northern Somali Current, 1995, *Geophys. Res. Lett.*, *24*(21), 2565–2568, 1997.

Semtner, A. J., and R. M. Chervin, A simulation of the global ocean circulation with resolved eddies, *J. Geophys. Res.*, *93*(C12), 15,502–15,522, 1988.

Semtner, A. J., and R. M. Chervin, Ocean general circulation from a global eddy-resolving model, *J. Geophys. Res.*, *97*(C4), 5493–5550, 1992.

Shetye, S. R., A. D. Gouveia, S. S. C. Shenoi, D. Sundar, G. S. Michael, A. M. Almeida, and K. Santanam, Hydrography and circulation off the west coast of India during the southwest monsoon 1987, *J. Mar. Res.*, *48*, 359–378, 1990.

Shetye, S. R., A. D. Gouveia, S. S. C. Shenoi, G. S. Michael, D. Sundar, A. M. Almeida, and K. Santanam, The coastal current off western India during the northeast monsoon, *Deep Sea Res., Part A*, *38*, 1517–1529, 1991.

Shetye, S. R., A. D. Gouveia, S. S. C. Shenoi, D. Sundar, G. S. Michael, and G. Nampoothiri, The western boundary current of the seasonal subtropical gyre in the Bay of Bengal, *J. Geophys. Res.*, *98*(C1), 945–954, 1993.

Stammer, D., R. Tokmakian, A. Semtner, and C. Wunsch, How well does a 1/4° global circulation model simulate large-scale oceanic observations?, *J. Geophys. Res.*, *101*(C10), 25,779–25,811, 1996.

Stramma, L., J. Fischer, and F. Schott, The flow field off southwest India at 8°N during the southwest monsoon of august 1993, *J. Mar. Res.*, *54*, 55–72, 1996.

Taft, B. A., and J. A. Knauss, The equatorial undercurrent of the Indian Ocean as observed by the Lusiad expedition, *Bull. Scripps Inst. Oceanogr.*, *9*, 163 pp., 1967.

Tsai, P. T. H., J. J. O'Brien, and M. E. Luther, The 26-day oscillation observed in the satellite sea surface temperature measurements in the equatorial western Indian Ocean, *J. Geophys. Res.*, *97*(C6), 9605–9618, 1992.

Visbeck, M., and J. Fischer, Sea surface conditions remotely sensed by upward-looking ADCPs, *J. Atmos. Oceanic Technol.*, *12*, 141–149, 1995.

Visbeck, M., and F. Schott, Analysis of seasonal current variations in the western equatorial Indian Ocean: Direct measurements and GFDL model comparison, *J. Phys. Oceanogr.*, *22*, 1112–1128, 1992.

Wyrtki, K., *Oceanographic Atlas of the International Indian Ocean Expedition*. 531 pp., Nat. Sci. Found., Washington, D.C., 1971.

Wyrtki, K., An equatorial jet in the Indian Ocean, *Science*, *181*, 262–264, 1973.

J. Fischer, J. Reppin, and F. A. Schott, Institut für Meereskunde an der Universität Kiel, Düsternbrooker Weg 20, 24105 Kiel, Germany. (e-mail: jfischer@ifm.uni-kiel.de; jreppin@ifm.uni-kiel.de; fschott@ifm.uni-kiel.de)

D. Quadfasel, Niels Bohr Institute for Astronomy, Physics and Geophysics, University of Copenhagen, Juliane Maries Vej 30, 2100 Copenhagen Ø, Denmark. (e-mail: dq@dcess.ku.dk)

(Received July 10, 1998; revised March 18, 1999; accepted March 26, 1999.)